Off-Center-Frequency Analysis of a Complete Planar Slotted-Waveguide Array Consisting of Subarrays

Jacob C. Coetzee, *Member, IEEE,* Johan Joubert, *Member, IEEE,* and Derek A. McNamara, *Senior Member, IEEE*

***Abstract*—An iterative procedure for calculating the off-center-frequency performance of a complete planar slotted-waveguide array, which consists of an arbitrary number of subarrays, is presented. The analysis includes the effects of the coupling slots from the main feed lines to the branch line guides, as well as the effects of RF manifolds, power slitters, or comparators used to distribute the power from the antenna input to the multiple subarray main lines. The procedure is applied to a large planar array for which dimensions have been obtained from an accurate metrology exercise. Good agreement between the predicted and measured performance of the array is demonstrated.**

***Index Terms*—Iterative methods, slot arrays, waveguide antennas.**

I. Introduction

SLOTTED-WAVEGUIDE arrays find wide application in communication and radar systems that require narrow-beam or shaped-beam radiation patterns, especially when high power, light weight, and limited scan volume are priorities [1]–[4]. Resonant arrays of longitudinal slots in the broad wall of rectangular waveguides have the added advantage of very low cross-polarization levels. Design procedures for these arrays are largely based on the work published by Elliott [5]–[7]. The slot spacing of such an array is one-half guide wavelength at the design frequency, so that the slots are located at the standing wave peaks. They radiate broadside beams, and all radiators have the same phase. Planar arrays are implemented using a number of rectangular waveguides (branch line guides), arranged side-by-side, while waveguides (main lines), which are located behind and at right angles to the branch lines, excite the radiating waveguides via centered-inclined coupling slots.

These arrays suffer from severe bandwidth limitations, and a usable bandwidth of a few percent is usually the norm. Various factors cause the off-center-frequency performance degradation. The frequency dependence of both the radiating slot properties and the coupling slot properties affects the excitation of the individual radiators. Frequency variations also cause the peaks of the standing waves to move significantly from the slot locations, resulting in phase differences in the slot fields. Various efforts have been made to reduce these effects. Techniques to improve the bandwidth of individual radiators include the use of wider slots and special slot geometries [8], and the reduction of the number of slots in waveguide sections through the use of subarrays [2]. In [2], guidelines for the expected bandwidth improvements that may be obtained by limiting the number of slots in any waveguide section are provided. However, this data is only approximate and does not take specific array geometries into consideration. Slotted-array seeker antennas also make use of subarraying, where a monopulse comparator network effectively feeds the four quadrants of the antenna either in-phase or out of phase with respect to each other [4]. An accurate analysis procedure would thus be useful for the prediction of the performance of monopulse arrays, and also in quantifying the effects that the implementation of subarraying have on the frequency performance of a planar array.

Hamadallah [9] proposed an analysis technique that is suitable for the theoretical calculation of linear slot-array performance parameters. An amended procedure, which includes the effects of higher order internal coupling between slots, was developed [10]. Neither of these procedures makes provision for the inclusion of the effects of the coupling slots between the main lines and the branch line guides of planar arrays. Details for doing this are provided in [11], but this procedure is only valid at the center frequency.

In this paper, an iterative procedure for the off-center-frequency analysis of a planar slotted-waveguide array consisting of an arbitrary number of subarrays, is presented. The formulation includes the frequency-dependent effects of the coupling slots, which is not a trivial extension of the center-frequency analysis. The influence of RF manifolds, power splitters, or comparators used to distribute the power from the antenna input to the multiple subarray main lines, is also accounted for. The procedure is applied to a large planar array for which dimensions have been obtained from a metrology exercise, and very good agreement between calculated and measured pattern performance is demonstrated.

II. Theory

A. Geometry

Consider a planar slot array consisting of a total of S subarrays. The sth subarray shown in Fig. 1 consists of a total of T_s branch lines, while the tth branch line has a total of $N_{s,t}$ slots. The slots are resonantly spaced, i.e., $d = \lambda_g/2$ and $d_0 = \lambda_g/4$ at the design frequency f_0. The subarray is fed by means of a main line, which is connected to the different branch line guides via centered-inclined coupling slots. The coupling-slot feeding branch line t of subarray s has an inclination angle of $\theta_{s,t}$ and a

Manuscript received October 23, 1998; revised June 30, 2000.

J. C. Coetzee is with the Department of Electrical and Computer Engineering, National University of Singapore, Singapore, 117576.

J. Joubert is with the Department of Electrical and Electronic Engineering, University of Pretoria, Pretoria 0002, South Africa.

D. A. McNamara is with the School of Information Technology and Engineering, University of Ottawa, Ottawa, ON K1N 6N5, Canada.

Publisher Item Identifier S 0018-926X(00)10834-8.

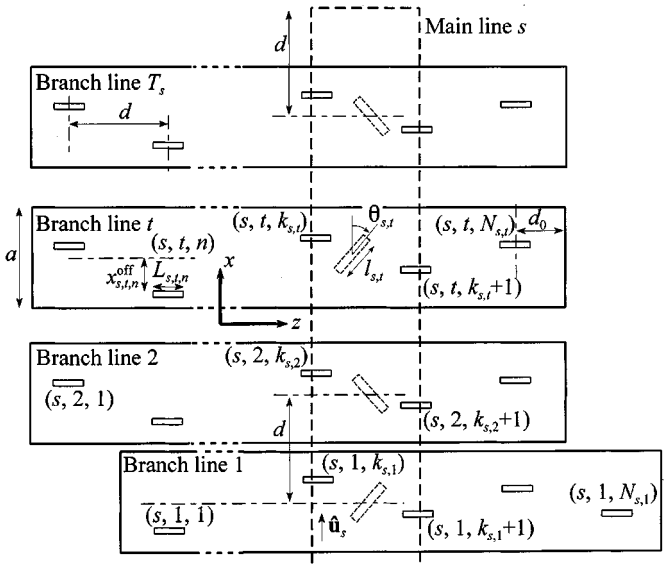

Fig. 1. Geometry of the sth subarray.

slot length of $l_{s,t}$. The angle $\theta_{s,t}$ is taken as positive in a clockwise direction, as measured from the positive x-axis. This coupling slot is located between the $k_{s,t}$th and the $(k_{s,t}+1)$th radiating slot of branch line t. The term $\hat{\mathbf{u}}_s = u_s\hat{\mathbf{x}}$ is the unit vector in the direction toward the shorted end of the main line, so that $u_s = \pm 1$ for subarrays fed from the bottom and the top, respectively. Two distinct radiating slot indexing conventions are used:

1) A local numbering system with a triple index (s, t, n) denoting slot n in branch line t of subarray s. The slot has a slot offset of $x^{\text{off}}_{s,t,n}$ relative to the center line of the branch line, and a slot length of $L_{s,t,n}$. Slots in a branch line are numbered from left to right, irrespective of whether the subarray is fed from the bottom (as in Fig. 1) or from the top. The branch lines are numbered such that the line closest to the feeding end is denoted by $t = 1$ and the line at the shorted end of the main line by $t = T_s$.
2) A global numbering system with a single index, i. The slot with local index (s, t, n) has a global index of

$$i = \sum_{u=1}^{s-1}\sum_{t=1}^{T_u} N_{u,t} + \sum_{v=1}^{t-1} N_{s,v} + n.$$

The complete array has a total number of

$$M = \sum_{s=1}^{S}\sum_{t=1}^{T_s} N_{s,t}$$

slots.

B. Equivalent Circuit for a Branch Line

The equivalent network for branch line t of subarray s is shown in Fig. 2, where $y^a_{s,t,n}$ is the normalized active admittance of the nth slot. The design procedure involves the repeated solution of a set of nonlinear equations in order to determine the slot offsets and lengths. The nonlinear equations are related to the so-called design equations, given by [6]

$$y^a_{s,t,n} = K_1 f_{s,t,n}\frac{V^{\text{slot}}_{s,t,n}}{V_{s,t,n}} \tag{1}$$

and [7]

$$\frac{1}{y^a_{s,t,n}} = \frac{1}{y^{\text{self}}_{s,t,n}} + \frac{1}{(f_{s,t,n})^2 K_2}\sum_{j=1,j\neq i}^{M}\frac{V^{\text{slot}}_j}{V^{\text{slot}}_i}\,g_{ji} + \frac{1}{(f_{s,t,n})^2 K_3} \cdot\left[\frac{V^{\text{slot}}_{s,t,n-1}}{V^{\text{slot}}_{s,t,n}}\,h_{s,t,n}h_{s,t,n-1} + \frac{V^{\text{slot}}_{s,t,n+1}}{V^{\text{slot}}_{s,t,n}}\,h_{s,t,n}h_{s,t,n+1}\right]. \tag{2}$$

For the slot with local index (s, t, n) and global index i, the slot voltage is denoted as $V^{\text{slot}}_{s,t,n}$ or V^{slot}_i, while the corresponding voltage on the equivalent network is $V_{s,t,n}$. The term $y^{\text{self}}_{s,t,n} = y^{\text{self}}(x^{\text{off}}_{s,t,n}, L_{s,t,n})$ represents the normalized self-impedance of this slot. It is calculated by applying a bivariate spline interpolation scheme on the precomputed slot data [12]. Both (1) and (2) remain valid at frequencies other than the design frequency. The terms g_{ji}, $f_{s,t,n}$, and $h_{s,t,n}$ are given by [6] and [7]. For the sake of completeness, and due to some differences in terminology, they are repeated here:

$$\begin{aligned} g_{ji} = {} & \int_{-k_0L_j/2}^{k_0L_j/2}\cos(\xi_j\lambda_0/2L_j) \\ & \cdot\left\{(\lambda_0/2L_i)\left[\frac{\exp(-jk_0R_1)}{k_0R_1} + \frac{\exp(-jk_0R_2)}{k_0R_2}\right]\right. \\ & + [1-(\lambda_0/2L_i)^2]\int_{-k_0L_i/2}^{k_0L_i/2} \\ & \left.\cdot\cos(\xi_i\lambda_0/2L_i)\frac{\exp(-jk_0R)}{k_0R}\,d\xi_i\right\}d\xi_j \end{aligned} \tag{3}$$

where

$$\begin{aligned} R_1 &= \sqrt{(x_j-x_i)^2 + [(z_j-z_i) + (\xi_j/k_0 - L_i/2)]^2} \\ R_2 &= \sqrt{(x_j-x_i)^2 + [(z_j-z_i) + (\xi_j/k_0 + L_i/2)]^2} \\ R &= \sqrt{(x_j-x_i)^2 + [(z_j-z_i) + (\xi_j/k_0 - \xi_i/k_0)]^2} \end{aligned} \tag{4}$$

and with (x_i, z_i) the coordinates of the center of the ith slot in the global coordinate system. Furthermore

$$\begin{aligned} f_{s,t,n} &= \frac{(\pi/kL_{s,t,n})\cos(\beta_{10}L_{s,t,n}/2)}{(\pi/kL_{s,t,n})^2 - (\beta_{10}/k)^2}\sin\left(\pi x^{\text{off}}_{s,t,n}/a\right) \\ h_{s,t,n} &= \frac{2(\lambda/2L_{s,t,n})\cosh[(\alpha_{20}/k)(kL_{s,t,n}/2)]}{(\lambda/2L_{s,t,n})^2 + (\alpha_{20}/k)^2} \\ &\quad\cdot\cos\left(2\pi x^{\text{off}}_{s,t,n}/a\right). \end{aligned} \tag{5}$$

β_{10} and α_{20} are the phase constant and attenuation constant of the TE_{10} and TE_{20} modes in the waveguide of width a, height b, and filled with a dielectric material of permittivity ϵ_r. The terms k_0 and k are the wavenumbers in free space and in the

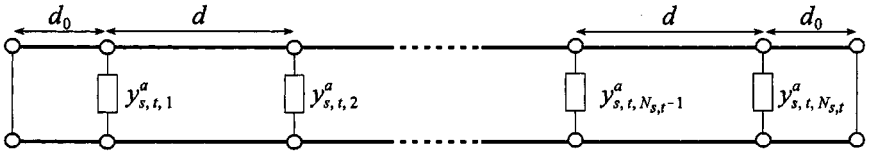

Fig. 2. Equivalent transmission line network for the tth branchline of the sth subarray.

dielectric, while λ_0 and λ are the corresponding wavelengths. The constants K_1, K_2, and K_3 are defined by

$$K_1 = \frac{1}{ja/\lambda}\sqrt{\frac{2Z_0 k/k_0}{\eta_0(\beta_{10}/k)(ka)(kb)}}$$
$$K_2 = \frac{2}{j(\beta_{10}/k)(k_0 b)(a/\lambda)^3}$$
$$K_3 = \frac{2(\alpha_{20}/k)}{j(\beta_{10}/k)}\exp(\alpha_{20}\, d) \tag{6}$$

where Z_0 is the arbitrary transmission-line characteristic impedance of the model in Fig. 2, while η_0 is the free-space intrinsic impedance. Although not explicitly stated in [7], the application of image theory reveals that for branch lines shorted at both ends, the terms $V^{\text{slot}}_{s,t,0}$, $V^{\text{slot}}_{s,t,N_{s,t}+1}$, $h_{s,t,0}$, and $h_{s,t,N_{s,t}+1}$ in (2) are given by

$$V^{\text{slot}}_{s,t,0} = -V^{\text{slot}}_{s,t,1} \qquad h_{s,t,0} = h_{s,t,1}$$
$$V^{\text{slot}}_{s,t,N_{s,t}+1} = -V^{\text{slot}}_{s,t,N_{s,t}} \qquad h_{s,t,N_{s,t}+1} = h_{t,N_{s,t}}. \tag{7}$$

C. Equivalent Circuit for a Main Line

Consider the crossed-guide coupler with inclination angle $\theta_{s,t}$ and slot length $l_{s,t}$ as shown in Fig. 3. The length of the coupling slot is usually chosen to be resonant at the design frequency. However, at an arbitrary frequency, the slots are no longer resonant. With each port terminated in a matched load, the scattering parameters of the coupler become

$$\begin{bmatrix} b_1^{(s,t)} \\ b_2^{(s,t)} \\ b_3^{(s,t)} \\ b_4^{(s,t)} \end{bmatrix} = \begin{bmatrix} S_{11}^{(s,t)} & 1-S_{11}^{(s,t)} & S_{31}^{(s,t)} & -S_{31}^{(s,t)} \\ 1-S_{11}^{(s,t)} & S_{11}^{(s,t)} & -S_{31}^{(s,t)} & S_{31}^{(s,t)} \\ S_{31}^{(s,t)} & -S_{31}^{(s,t)} & S_{33}^{(s,t)} & 1-S_{33}^{(s,t)} \\ -S_{31}^{(s,t)} & S_{31}^{(s,t)} & 1-S_{33}^{(s,t)} & S_{33}^{(s,t)} \end{bmatrix} \cdot \begin{bmatrix} a_1^{(s,t)} \\ a_2^{(s,t)} \\ a_3^{(s,t)} \\ a_4^{(s,t)} \end{bmatrix} \tag{8}$$

where $S_{11}^{(s,t)} = S_{11}(\theta_{s,t}, l_{s,t})$ and $S_{31}^{(s,t)} = S_{31}(\theta_{s,t}, l_{s,t})$ may be calculated by performing an interpolation scheme on precomputed data. Using the general relation between the scattering matrix elements of lossless networks, $S_{33}^{(s,t)}$ is obtained from

$$S_{33}^{(s,t)} = \frac{\text{Re}\left[S_{31}^{(s,t)}\right] - S_{31}^{(s,t)} S_{11}^{(s,t)^*}}{S_{31}^{(s,t)^*}}. \tag{9}$$

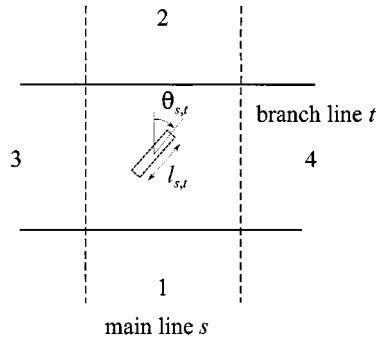

Fig. 3. Crossed-guide coupler geometry for the main line of the sth subarray and the tth branch line.

All network parameters are referenced to the center of the coupling slot.

Now consider the case where Ports 3 and 4 are terminated in normalized admittances $y_3^{(s,t)}$ and $y_4^{(s,t)}$. The corresponding reflection coefficients are then given by

$$\Gamma_3^{(s,t)} = \frac{1-y_3^{(s,t)}}{1+y_3^{(s,t)}}$$
$$\Gamma_4^{(s,t)} = \frac{1-y_4^{(s,t)}}{1+y_4^{(s,t)}}. \tag{10}$$

Therefore,

$$a_3^{(s,t)} = \Gamma_3^{(s,t)} b_3^{(s,t)}$$
$$a_4^{(s,t)} = \Gamma_4^{(s,t)} b_4^{(s,t)}. \tag{11}$$

Substitution of (11) into (8) yields the equivalent scattering parameters of the resulting two-port network, given by [13]

$$\begin{bmatrix} b_1^{(s,t)} \\ b_2^{(s,t)} \end{bmatrix} = \begin{bmatrix} S_{11}^{(s,t)} + R^{(s,t)} & 1-S_{11}^{(s,t)} - R^{(s,t)} \\ 1-S_{11}^{(s,t)} - R^{(s,t)} & S_{11}^{(s,t)} + R^{(s,t)} \end{bmatrix} \cdot \begin{bmatrix} a_1^{(s,t)} \\ a_2^{(s,t)} \end{bmatrix} \tag{12}$$

where

$$R^{(s,t)} = \left(S_{31}^{(s,t)}\right)^2 \cdot \frac{\Gamma_3^{(s,t)} + \Gamma_4^{(s,t)} - 2\Gamma_3^{(s,t)}\Gamma_4^{(s,t)}}{1-\Gamma_3^{(s,t)}\Gamma_4^{(s,t)} - S_{33}^{(s,t)}(\Gamma_3^{(s,t)} + \Gamma_4^{(s,t)} - 2\Gamma_3^{(s,t)}\Gamma_4^{(s,t)})}. \tag{13}$$

The expressions for the scattering parameters in (12) imply that the terminated crossed-guides coupler may be modeled as a series equivalent impedance, even at frequencies other than the

center frequency. The equivalent impedances shown in Fig. 4 may be calculated from

$$z^{(s,t)} = 2\frac{S_{11}^{(s,t)} + R^{(s,t)}}{1 - S_{11}^{(s,t)} - R^{(s,t)}}. \tag{14}$$

At the center frequency, (14) reduces to the simple expression for $z^{(s,t)}$ provided in [11].

D. Analysis of the Equivalent Circuits

Consider the equivalent circuit for branch line t of subarray s, as shown in Fig. 2. For $n > k_{s,t}$, the total normalized admittance as seen from the nth slot looking toward the right end of the branch line is obtained from the following recursive formulas:

$$\begin{aligned} y_{s,t,N_{s,t}}^{\text{tot}} &= y_{s,t,N_{s,t}}^{a} - j\cot(\beta_{10}d_0) \\ y_{s,t,n}^{\text{tot}} &= y_{s,t,n}^{a} + \frac{y_{s,t,n+1}^{\text{tot}}\cos(\beta_{10}d) + j\sin(\beta_{10}d)}{\cos(\beta_{10}d) + jy_{s,t,n+1}^{\text{tot}}\sin(\beta_{10}d)} \\ & \qquad n = (N_{s,t}-1),\,(N_{s,t}-2),\,\ldots(k_{s,t}+1). \end{aligned} \tag{15}$$

Similarly, for $n \le k_{s,t}$, the total normalized admittance as seen from slot n and looking toward the left end of the branch line, is given by

$$\begin{aligned} y_{s,t,1}^{\text{tot}} &= y_{s,t,1}^{a} - j\cot(\beta_{10}d_0) \\ y_{s,t,n}^{\text{tot}} &= y_{s,t,n}^{a} + \frac{y_{s,t,n-1}^{\text{tot}}\cos(\beta_{10}d) + j\sin(\beta_{10}d)}{\cos(\beta_{10}d) + jy_{s,t,n-1}^{\text{tot}}\sin(\beta_{10}d)} \\ & \qquad n = 2,\,3,\,\ldots k_{s,t}. \end{aligned} \tag{16}$$

The corresponding reflection coefficients as seen looking down the transmission line toward the left and right ends at the $k_{s,t}$th and the $(k_{s,t}+1)$th slots, respectively, are then given by

$$\begin{aligned} \Gamma_{s,t,k_{s,t}} &= \frac{1 - y_{s,t,k_{s,t}}^{\text{tot}}}{1 + y_{s,t,k_{s,t}}^{\text{tot}}} \\ \Gamma_{s,t,k_{s,t}+1} &= \frac{1 - y_{s,t,k_{s,t}+1}^{\text{tot}}}{1 + y_{s,t,k_{s,t}+1}^{\text{tot}}}. \end{aligned} \tag{17}$$

Transformed to the center of the coupling slot, these become

$$\begin{aligned} \Gamma_3^{(s,t)} &= \Gamma_{s,t,k_{s,t}}\exp(-j2\beta_{10}d_0) \\ \Gamma_4^{(s,t)} &= \Gamma_{s,t,k_{s,t}+1}\exp(-j2\beta_{10}d_0). \end{aligned} \tag{18}$$

The voltages on the equivalent transmission-line circuit referenced to the center of the coupling slot, are given by

$$\begin{aligned} V_3^{(s,t)} &= \frac{u_s S_{31}^{(s,t)}\left(1+\Gamma_3^{(s,t)}\right)\left(1-\Gamma_4^{(s,t)}\right)\sqrt{Z_0}\left(a_1^{(s,t)} - a_2^{(s,t)}\right)}{1-\Gamma_3^{(s,t)}\Gamma_4^{(s,t)} - S_{33}^{(s,t)}\left(\Gamma_3^{(s,t)} + \Gamma_4^{(s,t)} - 2\Gamma_3^{(s,t)}\Gamma_4^{(s,t)}\right)} \end{aligned} \tag{19}$$

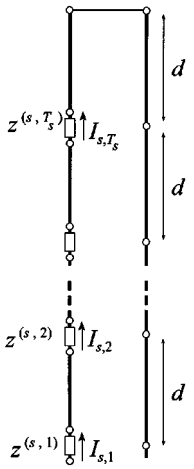

Fig. 4. Equivalent network for the main line of the sth subarray.

and

$$\begin{aligned} V_4^{(s,t)} &= -\frac{u_s S_{31}^{(s,t)}\left(1-\Gamma_3^{(s,t)}\right)\left(1+\Gamma_4^{(s,t)}\right)\sqrt{Z_0}\left(a_1^{(s,t)} - a_2^{(s,t)}\right)}{1-\Gamma_3^{(s,t)}\Gamma_4^{(s,t)} - S_{33}^{(s,t)}\left(\Gamma_3^{(s,t)} + \Gamma_4^{(s,t)} - 2\Gamma_3^{(s,t)}\Gamma_4^{(s,t)}\right)}. \end{aligned} \tag{20}$$

The voltages over the shunt elements in Fig. 2 are then given in terms of those in (19) and (20) by

$$\begin{aligned} V_{s,t,k_{s,t}} &= \frac{V_3^{(s,t)}}{\cos(\beta_{10}d_0) + jy_{s,t,k_{s,t}}^{\text{tot}}\sin(\beta_{10}d_0)} \\ V_{s,t,n} &= \frac{V_{s,t,n+1}}{\cos(\beta_{10}d) + jy_{s,t,n}^{\text{tot}}\sin(\beta_{10}d)} \\ & \qquad n = (k_{s,t}-1),\,(k_{s,t}-2),\,\ldots 1 \end{aligned} \tag{21}$$

and

$$\begin{aligned} V_{s,t,k_{s,t}+1} &= \frac{V_4^{(s,t)}}{\cos(\beta_{10}d_0) + jy_{s,t,k_{s,t}+1}^{\text{tot}}\sin(\beta_{10}d_0)} \\ V_{s,t,n} &= \frac{V_{s,t,n-1}}{\cos(\beta_{10}d) + jy_{s,t,n}^{\text{tot}}\sin(\beta_{10}d)} \\ & \qquad n = (k_{s,t}+2),\,(k_{s,t}+3),\,\ldots N_{s,t}. \end{aligned} \tag{22}$$

Refer to the equivalent circuit of the main line, shown in Fig. 4. The total normalized impedance as seen from the tth coupling slot looking toward the shorted end of the line is given by

$$\begin{aligned} z_{s,T_s}^{\text{tot}} &= z^{(s,t)} + j\tan(\phi_{\text{short}}) \\ z_{s,t}^{\text{tot}} &= z^{(s,t)} + \frac{z_{s,t+1}^{\text{tot}}\cos(\beta_{10}d) + j\sin(\beta_{10}d)}{\cos(\beta_{10}d) + jz_{s,t+1}^{\text{tot}}\sin(\beta_{10}d)} \\ & \qquad t = (T_s-1),\,(T_s-2),\,\ldots 1 \end{aligned} \tag{23}$$

where ϕ_{short} is the electrical length of the short-circuited section at the end of the main line (which might be a folded short if space limitations so require), and where $z^{(s,t)}$ is calculated using (14). The term $z_{s,1}^{\text{tot}}$, therefore, represents the input impedance of the sth main line, as seen from the first coupling slot. The input reflection coefficient for the sth main line is given by

$$\Gamma_{\text{in}}^{(s)} = \frac{z_{s,1}^{\text{tot}} - 1}{z_{s,1}^{\text{tot}} + 1}. \tag{24}$$

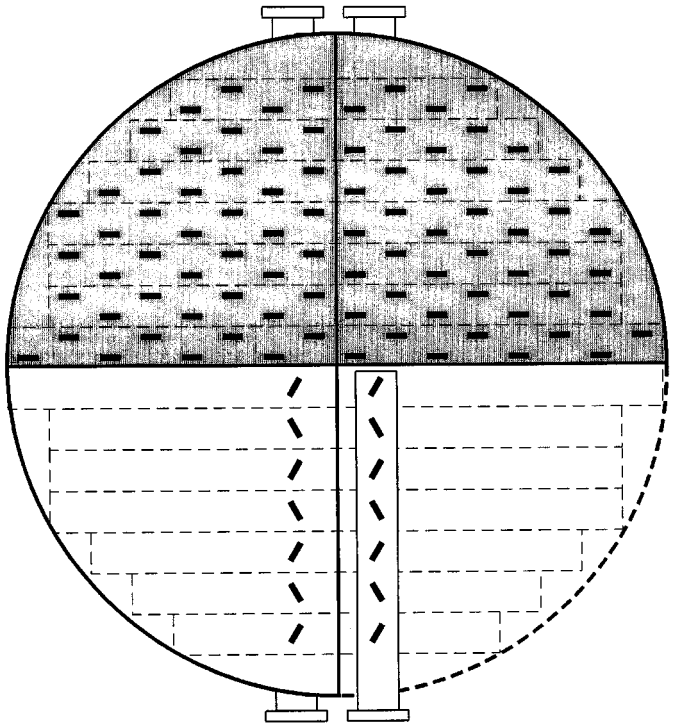

Fig. 5. Schematic representation of the physical array.

Furthermore,

$$\left(a_1^{(s,t)} - a_2^{(s,t)}\right) = \left(I_{s,t}\sqrt{Z_0}\right)\left(1 + z^{(s,t)}/2\right). \tag{25}$$

The current terms at the series impedances may be obtained from

$$\begin{aligned}\left(I_{s,1}\sqrt{Z_0}\right) &= \frac{2a_1^{(s,1)}}{z_{s,1}^{\text{tot}} + 1} \\ \left(I_{s,t}\sqrt{Z_0}\right) &= \frac{\left(I_{s,t-1}\sqrt{Z_0}\right)}{\cos(\beta_{10}d) + jz_{s,t}^{\text{tot}}\sin(\beta_{10}d)} \quad t = 2, 3, \ldots T_s.\end{aligned} \tag{26}$$

E. Modeling of Power Splitters or Comparators

An array consisting of a number of subarrays would naturally require some sort of a power-splitter network. This network distributes the power from the antenna input to the multiple subarray main lines. In general, an array consisting of S subarrays would require a splitter with $P = S + 1$ ports. For the sake of clarity, it is assumed that each of the first S ports is connected to its corresponding subarray, while the Pth port serves as the common feed port. From the definition of the scattering parameters, it follows that

$$\left[S^{\text{split}}\right][a] = [b] \tag{27}$$

$\left[S^{\text{split}}\right]$ is the $P \times P$ scattering parameter matrix of the network, specified with the phase reference of port 1 to port S at the center of the first coupling slot of the main line it is connected to. The elements of the scattering matrix are obtained either through measurement or analysis. However, the subarrays are not necessarily matched and consequently

$$a_s = \Gamma_{\text{in}}^{(s)} b_s \qquad s = 1, 2, \ldots S \tag{28}$$

with $\Gamma_{\text{in}}^{(s)}$ defined in (24). At the same time, it is true that

$$b_s = a_1^{(s,1)} \qquad s = 1, 2, \ldots S. \tag{29}$$

Substitution of (28) and (29) into (27) yields the following system of linear equations, from which the wave intensities incident at the first coupling slot of each main line may be calculated:

$$\begin{bmatrix} S_{11}^{\text{split}}\Gamma_{\text{in}}^{(1)} - 1 & S_{12}^{\text{split}}\Gamma_{\text{in}}^{(2)} & \cdot & S_{1S}^{\text{split}}\Gamma_{\text{in}}^{(S)} \\ S_{21}^{\text{split}}\Gamma_{\text{in}}^{(1)} & S_{22}^{\text{split}}\Gamma_{\text{in}}^{(2)} - 1 & \cdot & S_{2S}^{\text{split}}\Gamma_{\text{in}}^{(S)} \\ \cdot & \cdot & \cdot & \cdot \\ S_{S1}^{\text{split}}\Gamma_{\text{in}}^{(1)} & S_{S2}^{\text{split}}\Gamma_{\text{in}}^{(2)} & \cdot & S_{SS}^{\text{split}}\Gamma_{\text{in}}^{(S)} - 1 \end{bmatrix} \cdot \begin{bmatrix} a_1^{(1,1)} \\ a_1^{(2,1)} \\ \cdot \\ a_1^{(S,1)} \end{bmatrix} = \begin{bmatrix} -S_{1P}^{\text{split}} a_P \\ -S_{2P}^{\text{split}} a_P \\ \cdot \\ -S_{SP}^{\text{split}} a_P \end{bmatrix}. \tag{30}$$

The reflection coefficient at port P is given by

$$\Gamma = \frac{b_P}{a_P} = S_{PP}^{\text{split}} + \sum_{s=1}^{S} \frac{S_{Ps}^{\text{split}}\Gamma_{\text{in}}^{(s)} a_1^{(s,1)}}{a_P}. \tag{31}$$

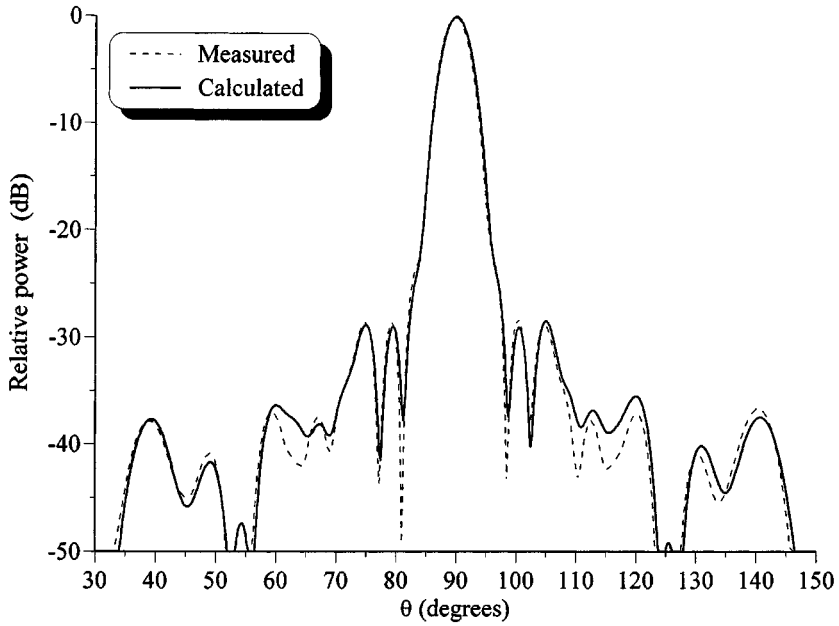

Fig. 6. Calculated and measured H-plane radiation pattern at a frequency of 8.8 GHz.

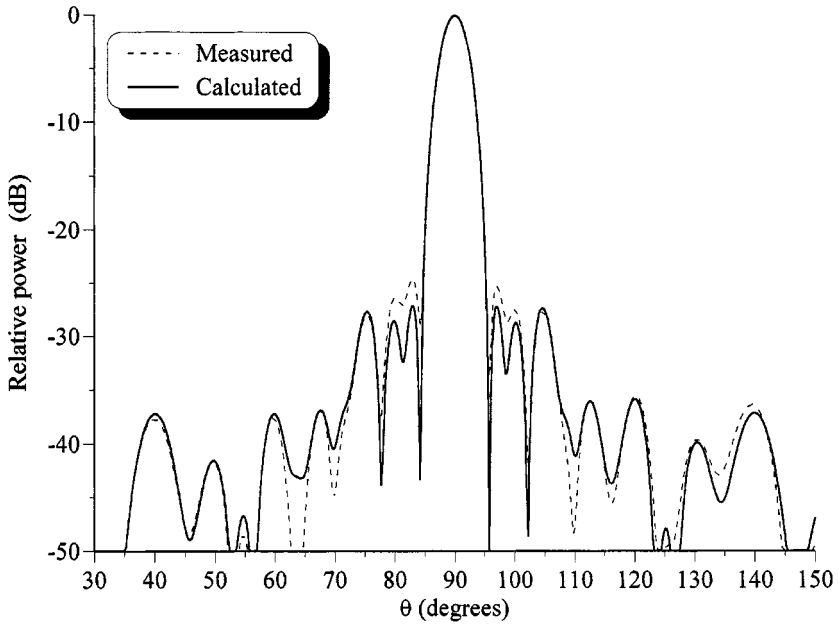

Fig. 7. Calculated and measured H-plane radiation pattern at a frequency of 8.9 GHz.

F. Analysis Procedure

By combining (1) and (2), the following set of linear equations is obtained:

$$K_2 \frac{(f_{s,t,n})^2}{y^{\text{self}}_{s,t,n}} V^{\text{slot}}_{s,t,n} + \sum_{j=1,\, j\neq i}^{M} V^{\text{slot}}_{j} g_{ji} + \frac{K_2}{K_3} \cdot \left[V^{\text{slot}}_{s,t,n-1} h_{s,t,n} h_{s,t,n-1} + V^{\text{slot}}_{s,t,n+1} h_{s,t,n} h_{s,t,n+1}\right] = \frac{K_2}{K_1} f_{s,t,n} V_{s,t,n} \quad s = 1, 2, \ldots S; \quad t = 1, 2, \ldots T_s; \quad n = 1, 2, \ldots N_{s,t}. \tag{32}$$

This may be written in matrix notation as

$$\left\{[g] + \begin{bmatrix} [H_{(1,1)}] & [0] & \cdot & [0] \\ [0] & [H_{(1,2)}] & \cdot & [0] \\ \cdot & \cdot & \cdot & \cdot \\ [0] & [0] & \cdot & [H_{(S,T_S)}] \end{bmatrix}\right\} \cdot \begin{bmatrix} \left[V^{\text{slot}}_{(1,1)}\right] \\ \left[V^{\text{slot}}_{(1,2)}\right] \\ \cdot \\ \left[V^{\text{slot}}_{(S,T_S)}\right] \end{bmatrix} = \begin{bmatrix} [U_{(1,1)}] \\ [U_{(1,2)}] \\ \cdot \\ [U_{(S,T_S)}] \end{bmatrix}. \tag{33}$$

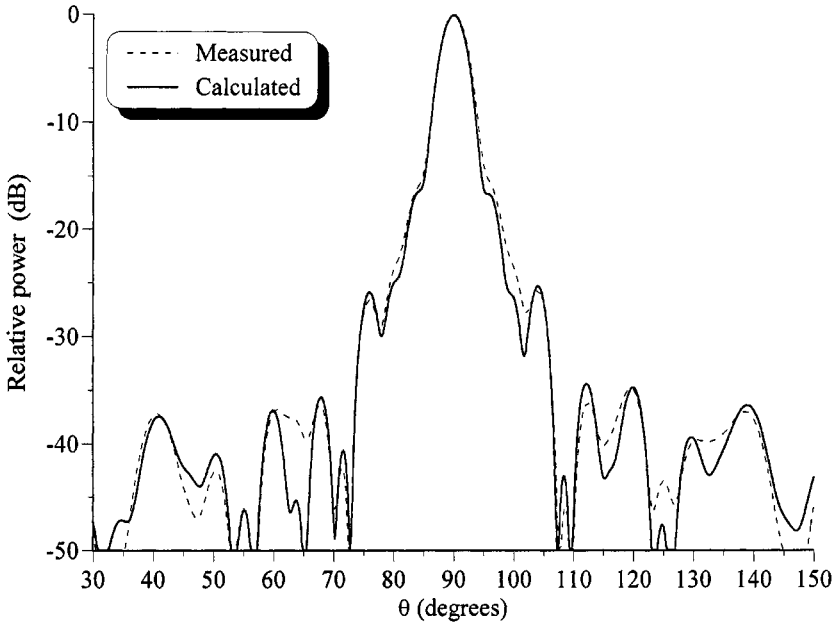

Fig. 8. Calculated and measured H-plane radiation pattern at a frequency of 9 GHz.

The term $[g]$ is a square $M \times M$ matrix with elements g_{ji} and where $g_{jj} = 0$. Submatrix $[H_{(s,t)}]$ is a square $N_{s,t} \times N_{s,t}$ matrix, with its elements given by

$$H_{(s,t)mn} = \begin{cases} \dfrac{K_2 (f_{s,t,m})^2}{y^{\text{self}}_{s,t,m}} & m = n,\ m \neq 1,\ m \neq N_{s,t} \\ \dfrac{K_2 (f_{s,t,m})^2}{y^{\text{self}}_{s,t,m}} - \dfrac{K_2 (h_{s,t,m})^2}{K_3} & m = n = 1;\ m = n = N_{s,t} \\ \dfrac{K_2 h_{s,t,m} h_{s,t,n}}{K_3} & |m-n| = 1 \\ 0 & |m-n| > 1 \end{cases} \tag{34}$$

$[V^{\text{slot}}_{(s,t)}]$ and $[U_{(s,t)}]$ are column vectors of dimension $N_{s,t}$, where the former represents the unknown slot voltages in branch line t of subarray s, while the components of the latter are defined by

$$U_{(s,t)m} = \frac{K_2 f_{s,t,m} V_{s,t,m}}{K_1}. \tag{35}$$

As in [9], an iterative approach may be followed in order to calculate the slot voltage as a function of frequency. The number of subarrays S, branch lines per subarray T_s, and slots per branch line $N_{s,t}$, are assumed to be specified. The offsets, lengths, and global coordinates for radiating slots, as well as the inclination angles and lengths for the coupling slots are also required. Additionally, the waveguide dimensions, interelement spacing d, radiating slot width w, unit vector component u_s for each subarray, and the index $n = k_{s,t}$ for each branch line, are to be specified. At each frequency point, the steps of the iterative analysis procedure are as follows.

1) Obtain $y^{\text{self}}_{s,t,n}$ for all radiating slots, and $S^{(s,t)}_{11}$, $S^{(s,t)}_{31}$ and $S^{(s,t)}_{33}$ for all coupling slots.
2) Calculate the elements g_{ji} using (3).
3) Assume initial values $y^{a}_{s,t,n} = y^{\text{self}}_{s,t,n}$.
4) Calculate $y^{\text{tot}}_{s,t,n}$ using (15) and (16).
5) From (17) and (18), calculate $\Gamma^{(s,t)}_3$ and $\Gamma^{(s,t)}_4$.
6) Calculate $R^{(s,t)}$ and $z^{(s,t)}$ using (13) and (14).
7) Calculate $z^{\text{tot}}_{s,t}$ using the recursive relations given in (23).
8) Compute $\Gamma^{(s)}_{\text{in}}$ from (24).
9) Determine the values of $a^{(s,1)}_1$ by setting $a_P = 1$ and solving the system of linear equations defined in (30).
10) Calculate $(I_{s,t}\sqrt{Z_0})$ using (26).
11) From (25), obtain values for $(a^{(s,t)}_1 - a^{(s,t)}_2)$.
12) Compute $V^{(s,t)}_3$ and $V^{(s,t)}_4$ from (19) and (20).
13) Calculate $V_{s,t,n}$ using (21) and (22).
14) Solve the system of linear equations defined in (33)–(35) for the unknowns $V^{\text{slot}}_{s,t,n}$.
15) Use the new values for $V^{\text{slot}}_{s,t,n}$ and recalculate $y^{a}_{s,t,n}$ using (2).
16) Repeat steps 4 to 15 until the values for $V^{\text{slot}}_{s,t,n}$ converge.
17) Calculate the input reflection coefficient of the entire array using (31).

Six to eight iterations are usually sufficient to ensure convergence for $V^{\text{slot}}_{s,t,n}$.

Note that at each frequency point at which the array performance is to be evaluated, a database of the self-impedance properties of isolated radiating slots and the scattering parameters for the crossed-guide coupler is required. An alternative approach is to gather this data only at a number of distinct frequencies, and to use a higher order interpolation scheme to calculate the self-impedances and scattering parameters in order to analyze the array at frequency points where slot data has not been generated explicitly.

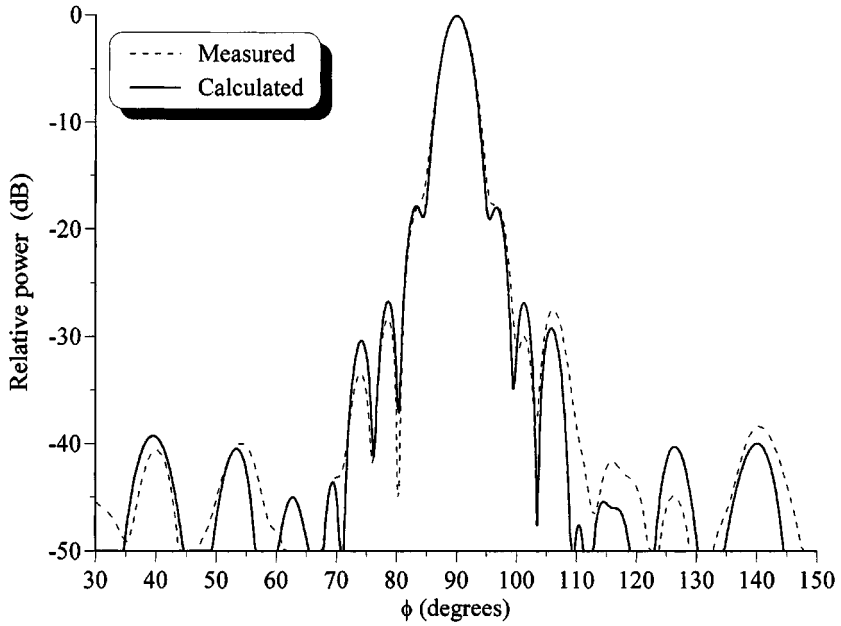

Fig. 9. Calculated and measured E-plane radiation pattern at a frequency of 8.8 GHz.

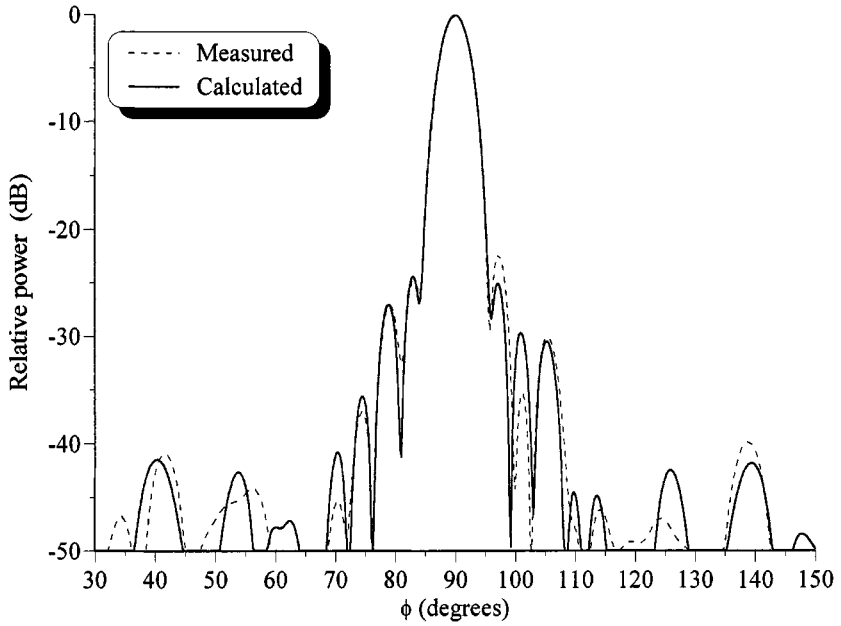

Fig. 10. Calculated and measured E-plane radiation pattern at a frequency of 8.9 GHz.

G. Calculation of the Radiation Patterns and Gain

Once the slot voltages are known, the radiation pattern of the array may be calculated. For this purpose, a piecewise sinusoidal approximation for the slot electric fields is used, which simplifies the expression for the radiated fields to

$$E_\phi(\theta,\phi) = \sum_{i=1}^{M} \frac{V_i^{\text{slot}}}{j\pi} F(k_0 L_i/2,\, \theta)\, \frac{\sin[k_0 \sin(\theta)\cos(\phi) w/2]}{k_0 \sin(\theta)\cos(\phi) w/2} \cdot \exp[jk_0(x_i \sin\theta\cos\phi + z_i \cos\theta)] \tag{36}$$

where

$$F(c,\theta) = \frac{\cos[c\cos(\theta)] - \cos(c)}{\sin(\theta)}. \tag{37}$$

The gain in the direction $(\theta_0,\, \phi_0)$ may be approximated by

$$G(\theta_0,\, \phi_0) = \frac{4\pi(1-|\Gamma|^2)|E_\phi(\theta_0,\, \phi_0)|^2}{\int_0^\pi \int_0^\pi |E_\phi(\theta,\, \phi)|^2 \sin\theta\, d\theta\, d\phi}. \tag{38}$$

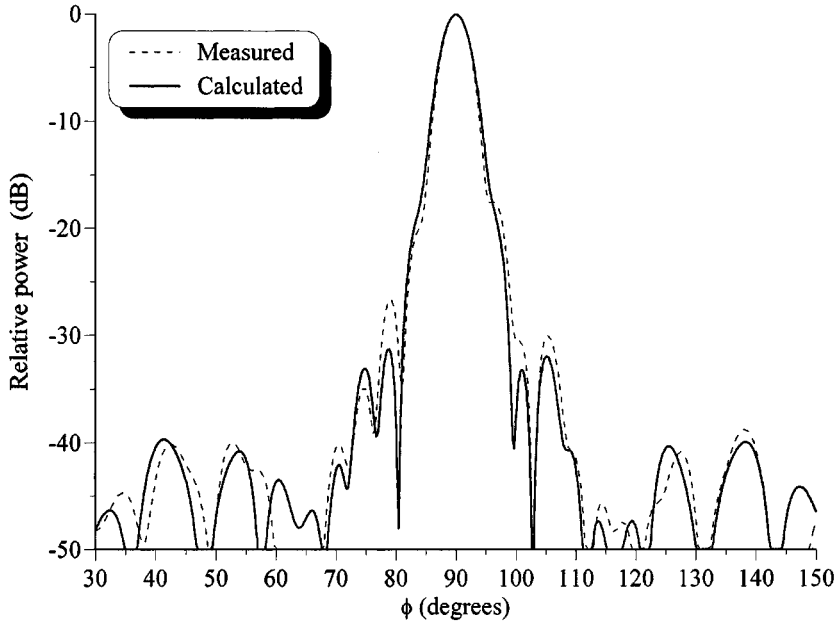

Fig. 11. Calculated and measured E-plane radiation pattern at a frequency of 9 GHz.

III. Results

The analysis procedure was applied to an existing planar array consisting of four subarrays, and with 312 radiating slots, similar to the antenna depicted in Fig. 5. The array was originally designed to operate at a frequency of 8.9 GHz. The array dimensions were obtained from an accurate metrology exercise. The method described in [14] was used to generate a database for the network model elements of isolated, rectangular radiating slots. The array had roundended slots, and a correction factor [15] was used to account for this. The scattering parameters for the inclined feeding slots were calculated using the method described in [13]. The coupling slots of the physical array were also roundended. For lack of a suitable correction factor, an assumption was made and the factor derived for radiating slots was again used. The splitter network, which fed the four subarrays, was assumed to be ideal. The radiation patterns in both the H-plane ($\phi = 90°$ and $30° \leq \theta \leq 150°$) and the E-plane ($\theta = 90°$ and $30° \leq \phi \leq 150°$) were calculated at frequencies of 8.8 GHz, 8.9 GHz, and 9 GHz. The theoretical results are compared to experimental data in Figs. 6–11. The agreement between the predicted and measured pattern performance in the H-plane is excellent. The correlation between calculated and measured E-plane radiation patterns is high, but minor deviations in the sidelobes might be ascribed to errors arising from the use of the untested correction factor for the lengths of the round-ended coupling slots. These errors would intuitively affect the E-plane radiation pattern more severely than it would in the case of the H-plane pattern. Note that commercially available finite-element analysis software is also suitable for the generation of data on the properties of the radiating and coupling slots [16]. Although the finite element software may not be as computationally efficient as the integral equation techniques, it does offer the possibility of a more direct analysis of round-ended slots. The proposed analysis procedure does not include the effects of higher order-mode coupling between coupling slots and the two radiating slots straddling them, which may be an additional source of error [11]. Calculated values for the on-axis gain are slightly optimistic, though within an acceptable tolerance range. Since the theoretical formulation is based on the assumption that the antenna is lossless, this is to be expected. For example, at the center frequency the gain was calculated as 32.3 dB, while a value of 31.5 dB was measured.

IV. Conclusion

An iterative procedure for the off-center-frequency analysis of a planar slotted-waveguide array consisting of an arbitrary number of subarrays was presented. The formulation includes the frequency-dependent effects of the main line to branch line couplers, and also of the power splitters responsible for the distribution of RF power to the main lines. Very good agreement between the predicted and measured pattern performance of a large slot array was demonstrated. The procedure may be employed for the accurate analysis of monopulse arrays in either the sum or the difference modes, merely by adjusting the parameters of the comparator network. It should also be useful in deciding between different geometries for an array when attempting to maximize the bandwidth of the antenna.

Acknowledgment

The authors wish to thank Dr. A. J. Booysen of Avitronics, Centurion, South Africa, who supplied the metrology data and the measured performance of the planar array.

References

[1] L. Sikora and J. Womack, "The art and science of manufacturing waveguide slot-array antennas," *Microwave J.*, pp. 157–162, June 1988.
[2] P. N. Richardson and H. Y. Lee, "Design and analysis of slotted waveguide arrays," *Microwave J.*, pp. 109–125, June 1988.
[3] J. Cross, D. Collier, and L. Goldstone, "Single slotted array achieves multimode performance," *Microwaves RF*, pp. 118–126, Apr. 1991.

[4] R. A. Sparks, "Systems applications of mechanically scanned slotted array antennas," *Microwave J.*, pp. 30–48, June 1988.
[5] R. S. Elliott and L. A. Kurtz, "The design of small slot arrays," *IEEE Trans. Antennas Propagat.*, vol. AP-26, pp. 214–219, Mar. 1978.
[6] R. S. Elliott, "An improved design procedure for small arrays of shunt slots," *IEEE Trans. Antennas Propagat.*, vol. AP-31, pp. 48–53, Jan. 1983.
[7] R. S. Elliott and W. R. O'Loughlin, "The design of slot arrays including internal mutual coupling," *IEEE Trans. Antennas Propagat.*, vol. AP-34, pp. 1149–1154, Sept. 1986.
[8] P. K. Park and I.P. Yu, "Characterization of dumbbell slots in rectangular waveguide by method of moments," in *Proc. 1984 Antennas Applications Symp.*, IL, Sept. 1984, pp. 1–6.
[9] M. Hamadallah, "Frequency limitations on broad-band performance of shunt slot arrays," *IEEE Trans. Antennas Propagat.*, vol. 37, pp. 817–823, July 1989.
[10] J. C. Coetzee and J. Joubert, "The effect of the inclusion of higher order internal coupling on waveguide slot array performance," *Microwave Opt. Tech. Lett.*, vol. 17, pp. 76–81, Feb. 1998.
[11] R. S. Elliott, "The design of waveguide-fed slot arrays," in *Antenna Handbook*, Y. T. Lo and S. W. Lee, Eds. New York: Van Nostrand Rheinhold, 1988.
[12] D. A. McNamara and J. Joubert, "On the use of bivariate spline interpolation of slot data in the design of slotted waveguide arrays," *ACES J.*, vol. 9, no. 1, pp. 6–9, 1994.
[13] W. Hanyang and W. Wei, "Moment method analysis of a feeding system in a slotted-waveguide antenna," *IEE Proc. H Microwaves, Antenna Propagat.*, vol. 135, pp. 313–318, Oct. 1988.
[14] J. Joubert and D. A. McNamara, "The analysis of radiating slots in rectangular waveguide inhomogeneously loaded with a dielectric slab," *IEEE Trans. Antennas Propagat.*, vol. 41, pp. 1212–1221, Sept. 1993.
[15] L. G. Josefsson, "Analysis of longitudinal slots in rectangular waveguide," *IEEE Trans. Antennas Propagat.*, vol. 35, pp. 1351–1357, Dec. 1989.
[16] K. W. Brown, "Design of waveguide slotted arrays using commercially available finite element analysis software," in *Proc. IEEE AP-S Int. Symp. Dig.*, Baltimore, MD, 1996, pp. 1000–1003.

Jacob C. Coetzee (M'94) was born in Pretoria, South Africa, in 1964. He received the B.Eng. and M.Eng. degrees (both with honors) in 1987 and 1989 and the Ph.D. degree in 1994, all from the University of Pretoria.

He served as a Senior Lecturer and Associate Professor in the Department of Electrical and Electronic Engineering of the University of Pretoria from 1994 to 1997. He joined the National University of Singapore as Assistant Professor in 1998. His research interests include computational electromagnetics and the analysis and the synthesis of passive microwave circuits and antennas.

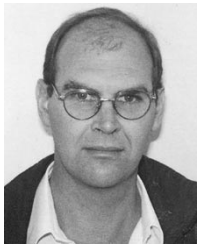

Johan Joubert (M'86) received the B.Eng, M.Eng, and Ph.D. degrees in electronic engineering from the University of Pretoria, Pretoria, South Africa, in 1983, 1987, and 1991, respectively.

From 1984 to 1988, he was a Research Engineer with the National Institute for Aeronautical and Systems Technology, Council for Scientific and Industrial Research, Pretoria, South Africa. In May 1988, he joined the Department of Electrical and Electronic Engineering, University of Pretoria, where he is currently a Professor of Electromagnetism. From July to December 1995, he was a Visiting Scholar in the Department of Electrical and Computer Engineering, California State University, Northridge, USA. His research interests include computational electromagnetism and the analysis and design of passive microwave components and antenna arrays.

Derek A. McNamara (S'79–M'81–SM'90) received the B.Sc. degree, with honors, from the University of Cape Town (UCT) in 1976, the M.Sc. degree from the Ohio State University in 1980, and the Ph.D. degree from UCT in 1986, all in electrical engineering.

During the periods 1977 to 1979 and 1981 to 1985, he was employed as a Senior Research Engineer at the Council for Scientific and Industrial Research (CSIR), Pretoria, South Africa. He was a Professor in the Department of Electrical and Electronic Engineering of the University of Pretoria from 1985 to 1994 and, in 1992, he was a Visiting Scientist at the *Institut für Höchsfrequenztechnik and Elektronik* (IHE) at the University of Karlsruhe, Germany. He was Principal Member of Technical Staff with the COM DEV Space Group, Ontario, Canada from 1994 through April 2000, from which time he has been a Professor in the School of Information Technology and Engineering (SITE), University of Ottawa, Canada. His present interests include antenna synthesis and design, computational electromagnetism, and the effective teaching of electromagnetic engineering. He is coauthor of the text *Introduction to the Uniform Geometrical Theory of Diffracation* (Norwood, MA: Artech House, 1990).